NANO LETTERS

Letter

pubs.acs.org/NanoLett

Manipulating Connectivity and Electrical Conductivity in Metallic Nanowire Networks

Peter N. Nirmalraj,[†,§,∥] Allen T. Bellew,[†,§] Alan P. Bell,[†,§] Jessamyn A. Fairfield,[†,§] Eoin K. McCarthy,[†,§] Curtis O'Kelly,[†,§] Luiz F. C. Pereira,[‡,§] Sophie Sorel,[‡,§] Diana Morosan,[‡,§] Jonathan N. Coleman,[‡,§] Mauro S. Ferreira,[‡,§] and John J. Boland*[,†,§]

[†]School of Chemistry, Trinity College Dublin, Dublin 2, Ireland

[‡]School of Physics, Trinity College Dublin, Dublin 2, Ireland

[§]Center for Research on Adaptive Nanostructures and Nanodevices, Trinity College Dublin, Dublin 2, Ireland

Supporting Information

ABSTRACT: Connectivity in metallic nanowire networks with resistive junctions is manipulated by applying an electric field to create materials with tunable electrical conductivity. In situ electron microscope and electrical measurements visualize the activation and evolution of connectivity within these networks. Modeling nanowire networks, having a distribution of junction breakdown voltages, reveals universal scaling behavior applicable to all network materials. We demonstrate how local connectivity within these networks can be programmed and discuss material and device applications.

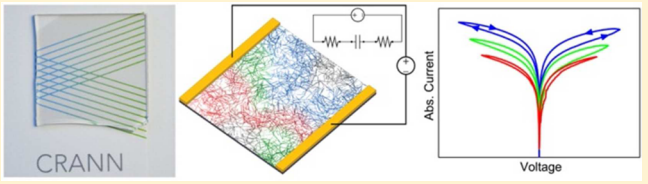

KEYWORDS: *Nanowire, network, conductivity, tunable*

While nanoscale materials have found applications in areas of devices,[1] sensors,[2] displays,[3] and medical technologies,[4] early efforts to exploit the potential of individual wires have met with limited success due to property variations and challenges associated with placement.[5] Consequently, there has been a growing interest in the use of random nanowire networks (NWNs),[6,7] where placement is not important and differences in properties are averaged out. These advantages, in combination with superior mechanical performance[8] and the ability to spray-deposit networks over large areas,[9] have extended potential applications to include transparent, flexible conductors[8,10] or even artificial skin.[11−13]

The global properties of any NWN are controlled by the connectivity between individual wires, which in turn depends on properties of the interwire junctions such as surface coating, work function, and contact geometry. Connectivity determines how information or charge is carried across the NWN from an array of electrodes that contact and interrogate it. Early studies addressed the onset of conduction and the formation of a percolation channel across ultrasparse wire networks or composites.[14,15] Here, we investigate NWNs comprised of Ag wires (individually coated with a nanoscale polymer passivation layer) and Ni wires with a passivating oxide (see S1, Supporting Information). While the former is qualitatively similar to earlier studies of nanoparticle and nanowire/polymer composites,[15,16] the network densities employed here are well beyond the percolation threshold. The latter is prototypical of non-noble (Cu, Ni, Co) NW systems. Several strategies have been reported to increase the conductivity of such networks. For example, the conductivity in Ag NWNs has been improved by using light−plasmon interactions to weld junctions,[17] but this method is applicable only to noble metals (Ag, Au, etc). The conductivity and stability of metal NWNs has also been improved by creating core−shell NW structures, such as Ni on Cu, that lead to oxidation resistant networks.[18]

Here we report for the first time observations of tunable connectivity and conductivity within the same material system, in contrast with previous studies where conductivity was controlled by changing the volume fraction of conducting nanomaterials.[19,20] Under the action of an applied electric field, the resistive junctions in our NWNs undergo breakdown that activates electrical conduction within the network. We find that connectivity evolves under electrical stressing to create materials with controllable conductivity. The voltage threshold for network activation exhibits a unique scaling behavior, which theory and simulation reveal to be consistent with a random distribution of junction properties. Our theory predicts the same scaling for all resistive junction networks, independent of the nanowire material or surface coating. We confirm this prediction by comparing the behaviors and performance of Ag and Ni NWNs with different surface passivations.

Network films were formed by spray deposition of nanowires onto Si substrates coated with 300 nm of thermal oxide. The nanowires were poly(vinylpyrrolidone) (PVP) surface-coated Ag NWs (Seashell Technology) and surface-oxide-passivated Ni NWs (Nanomaterials.it), with an average NW length

Received: September 13, 2012
Revised: October 11, 2012

   dx.doi.org/10.1021/nl303416h | *Nano Lett.* XXXX, XXX, XXX−XXX

(diameter) of 7.3 μm (86 nm) and 9.4 μm (80 nm), respectively (see S1). Ti/Au and Pd contact electrodes, deposited using a shadow mask, enabled transport measurements between pairs of electrodes at fixed separations or between a single electrode and a conducting atomic force microscopy (CAFM) probe. AFM probes act as mobile nanoscale contacts that can generate simultaneous topographic and conductance maps.[21−26] Previous studies used CAFM to analyze the junction resistance in SWCNTs,[22,26,27] graphene flake networks,[28] and contact resistances to metal electrodes.[29] The metal coated CAFM tips (Pt/Cr, 0.2 N/m, Cont E, Budget Sensors) employed a constant loading force of 1 nN and ∼2.5 nN, during imaging and local tip-induced electrical activation, respectively.

CAFM revealed that Ag NW networks do not conduct under low bias voltage conditions (200 mV) even when wires and electrodes are physically well coupled (Figure 1a). The PVP

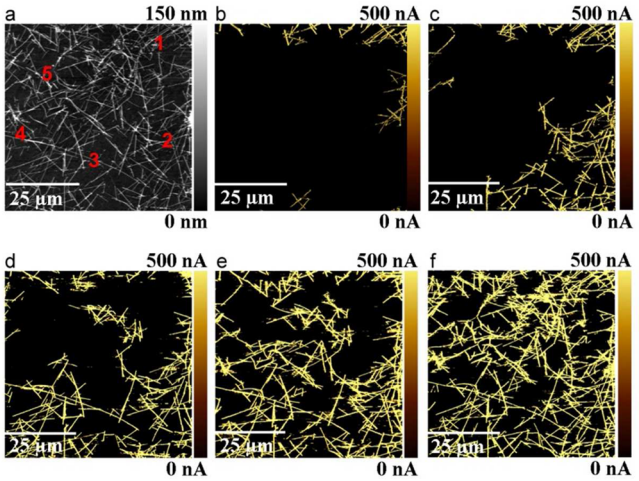

Figure 1. (a) Topography of a random network of Ag nanowires. The metal coated AFM tip was used to locally activate sites in the network by applying a voltage pulse of 6 V for ∼2 s and then imaging the same network region under a lower bias of 200 mV. The current maps shown in b−f are a result of applying the voltage pulses at selected regions marked 1−5 on the topographic map. The network can be seen to turn on locally as the wires become connected to each other and to the electrode following local probe excitation. Note: the electrode is located at the top of the image.

surfactant layer impedes conduction, though it can be removed with heat treatment to yield conductivities as high as 5×10^6 S/m.[8] Increasing the tip-electrode bias in steps of 10 mV reveals the existence of a voltage threshold, V_T, for conduction. The NWN connectivity was then investigated by locally applying voltage pulses above V_T. Figure 1b shows the result of a 6 V, 2 s pulse at location 1 in Figure 1a, with the same area subsequently imaged at 200 mV. This region of the network is now connected to the Pd contact electrode (not shown but located at the top of the image). Repeating this process at locations 2 through 5 resulted in the current maps in Figure 1c−f, following which most but not all of the network became conducting.

The value of V_T depends on the distance from the electrode and the network density. Figure 2a shows typical $I-V$ curves measured for a sparse NWN with tip−electrode separations of 100 and 700 μm. Each $I-V$ measurement shows an abrupt threshold V_T that increases with the distance from the electrode, and the retrace shows that the network has been locally turned on. The observed increase in V_T with distance is consistent with an increased number of junctions that have to be broken down between the electrodes.

Figure 2b shows V_T as a function of tip−electrode separation for NWNs of different densities using large electrodes fabricated by a combination of lithography and shadow mask. The network density was measured optically (% transmission T at 550 nm) and transformed into the number of nanowires per unit area, N/A (see S2). V_T increases sharply but then is observed to level off beyond a certain distance from the electrode. The overall shape of the curve is similar regardless of density, except that the plateau value decreases as the network density increases, consistent with an increased number of parallel paths between the two electrodes. Whereas Figure 2b shows V_T as a function of D for various network densities, N/A, these data can be replotted to show V_T as a function of N/A for various values of D on a log−log scale (see S3). The resulting data are well-described by the power law $V_T \propto (N/A)^n$, and the measured exponents n are plotted as a function of D in Figure 2c. We note that the exponent n increases sharply from −1 at small D to −1/2 for larger tip-electrode separations. We now demonstrate that this scaling behavior is an intrinsic network property.

The electrical properties of the Ag NWN can be modeled as a leaky resistor−capacitor network with randomly distributed junctions, where $\rho(v_B)$ is the distribution of breakdown voltages v_B across individual junctions. We assume that the application of an applied voltage, V, results in the breakdown or activation of a certain number of weak junctions, regardless of whether this results in a continuous conducting path between electrodes. The total number of activated junctions per unit area of network is given by:

$$\frac{N_{J,B}}{A} = \frac{N_J}{A}\int_0^v dv_B \rho(v_B) \quad (1)$$

where v is the mean voltage across an individual junction and N_J/A is the total number of junctions per unit area. Furthermore, given the 2-D nature of the network, the average separation $\langle d_B \rangle$ between activated junctions is $\langle d_B \rangle \approx (A/N_{J,B})^{1/2}$, where A is the film area.

Simulations describing the existence of a voltage threshold for the onset of charge current were carried out by considering an ensemble of nanowires randomly distributed inside a two-dimensional box of arbitrary size. Any two neighboring wires should function as a capacitor that builds up a voltage difference across the junction. How the voltage is distributed across the system can be found by solving the Poisson equation for this random network of capacitors. Charge will only flow across any given junction if the voltage difference exceeds a certain threshold, which is also randomly distributed across the network. In this case, the junction experiences a capacitive breakdown, and the wires become activated. By mapping how the voltage is distributed across the junctions, we can address the conditions for activating the network both on a local as well as on a global scale. For global activation, the voltage threshold, V_T, is the voltage which results in activated junctions all the way between electrodes.

Our simulations reveal that activation of one junction can result in activation of nearby junctions resulting in a local cascade. Thus, cells of connected junctions of characteristic size R_c are created following the application of a voltage V and are bounded by higher barrier junctions that remain stable at this

dx.doi.org/10.1021/nl303416h | Nano Lett. XXXX, XXX, XXX−XXX

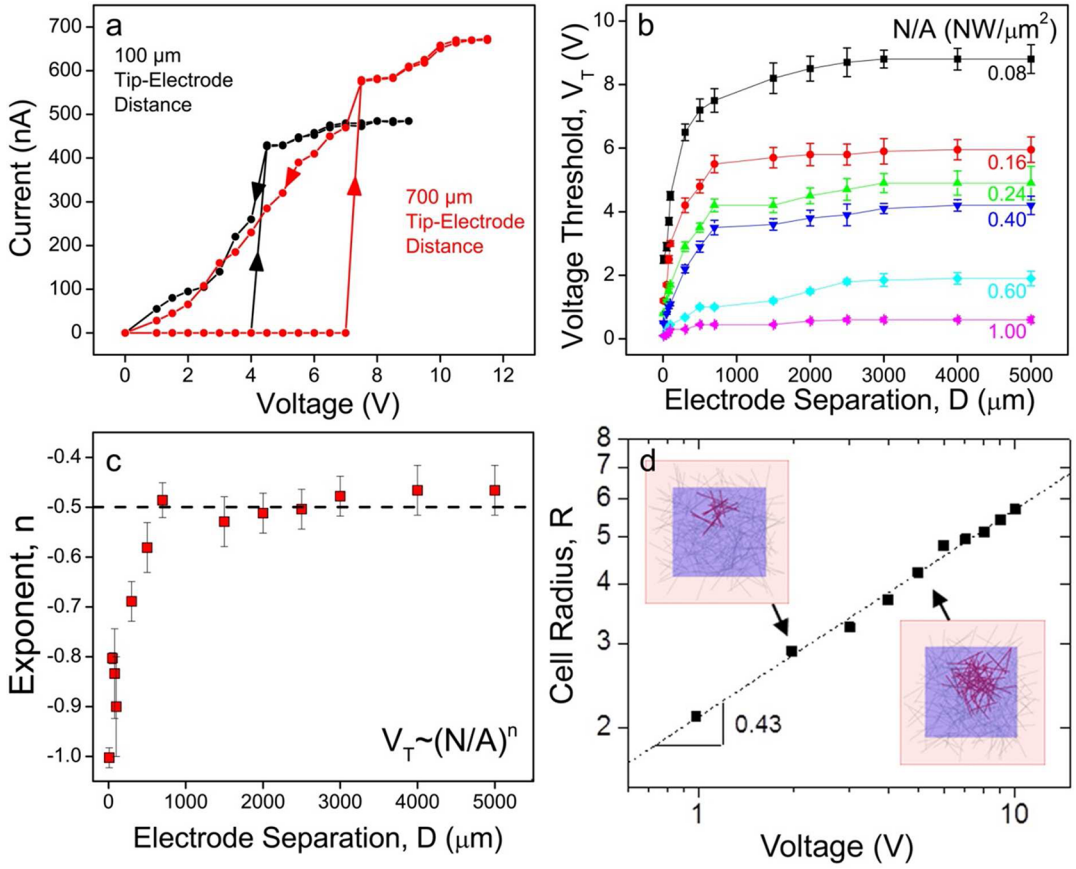

Figure 2. (a) Initial activation of a sparse Ag NWN at 100 μm (black curve) and 700 μm (red curve) electrode separations. (b) The variation of the voltage threshold for network activation as a function of electrode separation for different network densities (N/A). (c) The plot of the exponent n vs electrode separation D following the rescaling of the data in b as (see SI for additional details). (d) Simulated size of connectivity cell of nanowires plotted as a function of tip bias voltage.

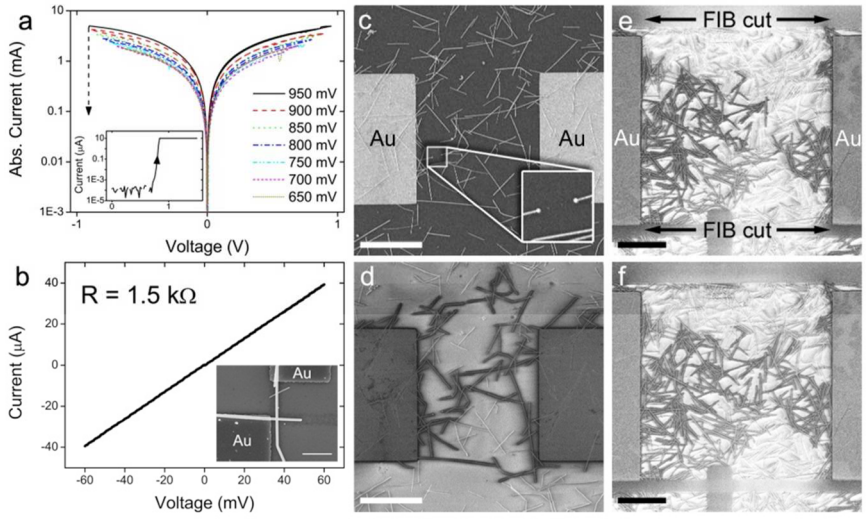

Figure 3. (a) $I-V$ curves with different V_{max} values for a sparse network ($T > 95\%$) at small electrode separations (20 μm) that ultimately fails (down arrow). (b) $I-V$ from a single junction (see inset) formed between two Ag NWs, showing a two-point resistance of 1.5 kΩ. (c) SEM and (d) passive voltage−contrast images of the failed network in A; inset indicates the failure point. (e) Initial activation and (f) formation of conducing path in a denser network ($T = 85\%$; $D = 40$ μm). FIB milling was used to isolate the region between the electrodes from the surrounding network. Scale bars are 10 μm.

voltage. We assume that R_c grows with V as a power law, such that $R_c = aV^{\alpha}$, where a and α are constants. A continuous conducting path is established between electrodes when enough junctions break down such that the connectivity cells overlap, or when $\langle d_B \rangle \approx R_c$, that is,

dx.doi.org/10.1021/nl303416h | Nano Lett. XXXX, XXX, XXX−XXX

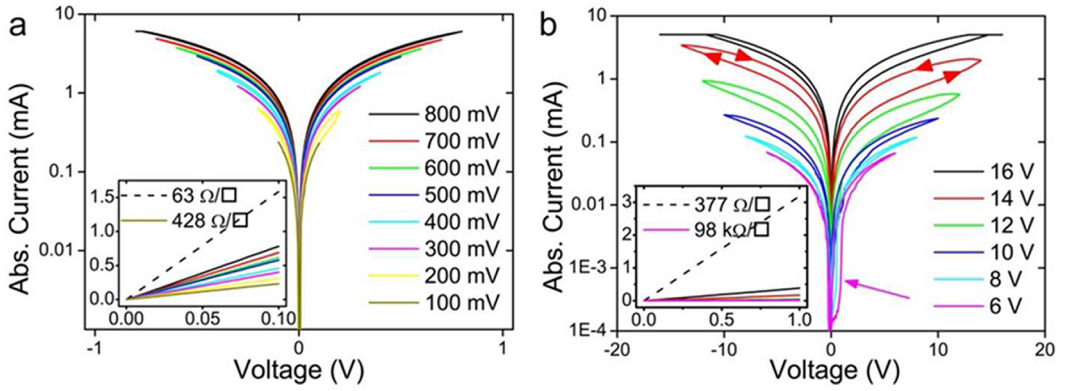

Figure 4. $I-V$ measurements with different V_{max} values for same T = 80% network with electrode separations of (a) 40 μm and (b) 1000 μm. In both cases the network was FIB-cut to eliminate contributions beyond the electrode gaps. Note both exhibit hysteresis and evolution of connectivity. The insets demonstrate ability to tune the network sheet resistance over a wide range. Full connectivity (i.e., lowest possible sheet resistance) can only be achieved in the case of part a; see the text. The arrow in part b identifies a sudden increase in connectivity.

$$aV_T^{\alpha} \approx \left[\eta \frac{N}{A} \int_0^{v} dv_B \rho(v_B)\right]^{-1/2} \quad (2)$$

where $N_J/A = \eta \times N/A$ and η is the mean number of junctions per wire. Note that V now becomes V_T because this condition describes the voltage threshold where an initial conducting path is formed and a current is measured between the two electrodes. Importantly, the network self-selects the lowest barrier junctions to establish this initial conducting path.

We can use eq 2 to obtain a relationship between V_T and N in the special case where D is very small. In this scenario, v must be relatively large and therefore close to the upper range of voltage values in the $\rho(v_B)$ distribution, so that a single connectivity cell spans the channel between electrodes, and we can approximate $\int_0^v dv_B \rho(v_B)$ as being v-independent. Since we know from experiment that $V_T \propto (N/A)^{-1}$ for small D, it must be the case that $\alpha = 1/2$. For the case of larger separations D, a similar analysis predicts $V_T \propto D^{1/3}$, which agrees with the data in Figure 2b (see S4). In this $n = -1/2$ regime, connectivity cells become linked together to establish the initial conducting path across the channel.

Electrostatic simulations of connectivity and cell formation were also performed. This involved modeling the network as a random distribution of junction capacitances and monitoring the response of the network to the increasing electric field created between a point probe electrode (simulating the AFM tip) and a distant far-field electrode. Figure 2d shows the growth of the connectivity cell with applied voltage. The simulations reveal that junction breakdown occurs most readily in the vicinity of the probe due to the increased electric field in this region. Crucially, we find that the size of the connectivity cell increases with the applied voltage as a power law with an exponent α = 0.43, which is in excellent agreement with the value of $\alpha = 1/2$ predicted by our theory.

Following activation, the behavior of the Ag NWN should depend on the number of junctions that remain *disconnected* from established conducting paths and hence depends on the overall network density. To test this, networks were activated by setting the current compliance to 10 μA following which $I-V$ curves were measured by sweeping the voltage over the range: $0 \rightarrow V_{max} \rightarrow 0 \rightarrow -V_{max} \rightarrow 0$. A large compliance insures a stable conducting path is established, but too large a value will mask changes in connectivity. Typically V_{max} was gradually increased to help visualize the evolution of the network connectivity.

Figure 3a shows $I-V$ measurements for a short-channel ultrasparse network (T > 95%, D = 20 μm) corresponding to the $n = -1$ regime. The inset shows the network activation step. The network conductivity is seen to continuously increase as the maximum sweep voltage, V_{max}, is increased up to the point of failure (down-arrow). To eliminate any possibility that this increase in conductivity is due to multistage activation behavior at individual junctions, the $I-V$ data from a *single* NW−NW junction is shown in Figure 3b, demonstrating that individual activated junctions are ohmic and free from hysteresis. The two-point resistance shown is 1.5 kΩ, but values as low as 180 Ω have been observed, these variations being due to the quality of the contact electrodes. Figure 3c,d show scanning electron microscope (SEM) and in-lens passive voltage contrast images of the failed network in Figure 3a. The network failure-point is indicated in Figure 3c. Passive voltage contrast imaging visualizes conducting paths within the network, where connected wires appear dark when at the same potential as the grounded electrodes.[30] We note that all wires physically bridging the electrodes are connected and that connectivity evolves to include wires beyond the gap area and even includes those that do not contribute to the current (see S5), in agreement with our model.

The activation process itself can also be visualized. Figure 3e,f shows the case of a low density network (T = 85%; D = 40 μm) that has been milled using a focused ion beam (FIB) to isolate the active device area from the nanowires outside it. This eliminates contributions from any part of the NWN outside the area between the electrodes and allows the sheet resistance to be accurately measured. During activation, Figure 3e shows that the wires are connected to the electrode and to each other but do not form a continuous conducting path. In agreement with theory, the connectivity cell eventually extends across the entire channel (Figure 3f), establishing a conducting path and enabling current flow. Additional electrical stressing activates the remaining wires, ultimately leading to a fully connected network.

We now consider the level of connectivity attainable for an Ag NWN. Figure 4a shows $I-V$ measurements for a short channel (T = 80%; D = 40 μm) FIB-cut network, where the connectivity evolves over a limited current range as V_{max} is increased. Figure 4b shows $I-V$ measurements for this *same*

dx.doi.org/10.1021/nl303416h | *Nano Lett.* XXXX, XXX, XXX−XXX

network (T = 80%) but with D = 1000 μm, corresponding to the n = −1/2 regime. The presence of pronounced hysteresis loops in Figure 4b, which are not as evident in Figure 4a, is due to the larger numbers of accessible junctions that can undergo breakdown at higher applied voltages, leading to the consolidation of existing conducting paths or the establishment of new ones. The hysteresis loops are larger at positive bias due to the direction of the voltage sweep used. I−V data in Figure 4b also evolve over a much larger current range and exhibit a sudden increase whenever a section of network becomes connected to an established path (see arrow in Figure 4b). More pronounced examples are shown in S6, which illustrates the time−voltage dependence of the hysteresis. Following preferential activation of the lowest barrier junctions to establish conducting pathways, increasing the voltage causes additional junctions to breakdown thus evolving the connectivity along and between these paths. These pathways are visualized as darkened tracks in voltage contrast images (see S7) and ultimately lead to the memristive-like behaviors in Figure 4a,b.

At low bias, connectivity evolves slowly, and networks can exhibit a range of stable conductivities. The lower bound is determined by the current compliance during activation, while the upper bound is controlled by the properties of the fully connected network. Our electronics are current limited (5 mA), and we cannot controllably saturate the hysteresis. However, manual activation and stressing of the T = 80% network yielded maximum sheet resistance values of 63 Ω/sq and 377 Ω/sq (see insets in Figure 4), when D = 40 μm and D = 1000 μm, respectively. The former is consistent with the 80 Ω/sq two-probe sheet resistance recorded for a 200 °C annealed pristine T = 80% network, demonstrating that for short channels (n = 1 regime) all junctions can be broken-down, leading to maximal connectivity. This is not possible at larger length-scales; measured sheet resistance values are typically 5−10× the minimum value, since the density of connectivity cells and conducting paths is too low for complete activation. However, activating pairs of electrodes in an array that spans the network may increase the numbers of such paths, thereby enhancing conductivity. Because network connectivity in these devices can be locally programmed, the use of electrode arrays and more complex electrode geometries is expected to enable other applications, for example neural networks where the weights (connections) between individual electrodes (inputs and outputs) can be manipulated.[31,32]

Although our experiments have largely focused on PVP-coated Ag NW networks, our theoretical model is applicable to all network materials with resistive junctions. To test this we performed measurements on Ni NWNs, comprised of wires with passivating oxides (see S1). Figure 5 shows that the Ni network (D = 600 μm, T = 80%) evolves connectivity and conductivity after the initial activation step (see left inset). The activation and operational voltage values are larger than for Ag, reflecting the more robust nature of the metal oxide passivation compared to PVP, and differences in the dielectric breakdown mechanism (see below). However, the connectivity and resulting conductivity evolves as was observed for the Ag NWN, and the inset shows the sheet resistance of the network can be tuned over a range of values. The lowest recorded sheet resistance is 36 kΩ/sq, indicating that the network has not been completely activated, as was also the case for the larger Ag NWNs in Figure 4b. Once again we anticipate that activation using an electrode array will enable the conductivity in different

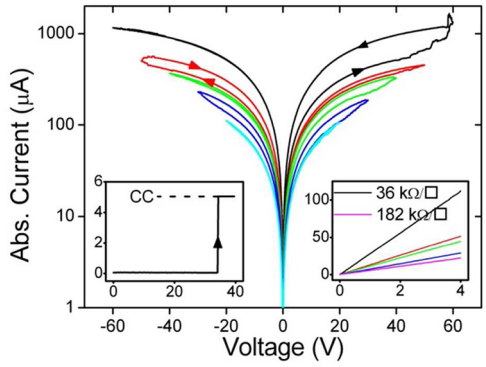

Figure 5. I−V measurements for a Ni NWN with T = 80%, D = 750 μm. Ni NWs with an oxide passivation layer display the same I−V behavior as that seen for Ag NWs. Once the network is activated (see inset on left), the conductivity of the network can be controlled by increasing the maximum sweep bias. As new paths are added, the network's conductivity increases (see inset on right). The voltages required are greater than in the case of Ag, reflecting the enhanced robustness of NiO and a different breakdown mechanism.

regions to be controlled or programmed, while at the same time enabling higher overall levels of connectivity and conductivity. It is also important to emphasize that the connections formed between wires are robust. Repeated measurements on activated networks exposed to ambient over an 8-week period reveal no degradation of the network conductivity. Electrical breakdown in planar Ni/NiO/Ni junctions have been extensively studied and involves the formation of conductive metallic Ni filaments through the oxide.[33,34] Presumably the same phenomenon also occurs in networks, and the surrounding oxide inhibits subsequent oxidation of the Ni filaments that control network connectivity.

In this Letter we have introduced a new mechanism to control connectivity and conductivity in nanoscale materials networks. We reported a scaling behavior that provides insights into the level of connectivity that is achievable and the ability to control connectivity on a local scale by simply addressing the network with local contact electrodes. This approach may also open up the possibility of exploiting low cost metal NWNs (e.g., Ni, Cu) for transparent conductor applications. In addition, we anticipate the possibility that different surface passivations or functionalizations and wire types may yield new types of network materials that respond to other external stimuli, such as light or magnetic fields.

■ ASSOCIATED CONTENT

Supporting Information

Characterization of Ag and Ni nanowires, conversion of the optical transmittance into number density of NWs, rescaling of the V_T vs D measurements, theoretical description of threshold behavior for the case of intermediate D, spatial evolution of connectivity, time dependence of connectivity evolution, and visualization of conduction paths in large-scale networks. This material is available free of charge via the Internet at http://pubs.acs.org.

■ AUTHOR INFORMATION

Corresponding Author

*E-mail: jboland@tcd.ie. Phone: +353 1-896-3140.

dx.doi.org/10.1021/nl303416h | Nano Lett. XXXX, XXX, XXX−XXX

Present Address

[‖]IBM Research Laboratories, Saumerstrasse 4, Ruschlikon, CH 8803, Zurich, Switzerland.

Notes

The authors declare no competing financial interest.

■ ACKNOWLEDGMENTS

We acknowledge the Science Foundation Ireland funded collaboration (SFI Grant 03/CE3/M406s1) and the SFI Principal Investigator (Grant No. 06/IN.1/I106) and CSET award which facilitated this work and INSPIRE for access to the Advanced Microscopy Laboratory. P.N.N. performed CAFM experiments on Ag NWs and recorded data for scaling. A.T.B. fabricated and electrically tested large channel networks. A.P.B. performed short channel experiments. J.A.F. performed SEM passive voltage contrast measurements. C.O.K. performed FIB cuts of network samples. E.K.M. performed TEM analysis of Ag networks. S.S. assisted in network spray deposition. L.F.C.P. and D.M. performed modeling and simulation. M.S.F. led the simulation team. J.N.C. led the processing team. J.J.B. led the overall effort, designed the experiments, and wrote the paper.

■ REFERENCES

(1) Aguirre, C. M.; Auvray, S.; Pigeon, S.; Izquierdo, R.; Desjardins, P.; Martel, R. *Appl. Phys. Lett.* **2006**, *88* (18), 183104−3.

(2) Allen, B. L.; Kichambare, P. D.; Star, A. *Adv. Mater.* **2007**, *19* (11), 1439−1451.

(3) Eda, G.; Fanchini, G.; Chhowalla, M. *Nat. Nanotechnol.* **2008**, *3* (5), 270−274.

(4) Baughman, R. H.; Zakhidov, A. A.; de Heer, W. A. *Science* **2002**, *297* (5582), 787−792.

(5) Langford, R. M.; Wang, T.-X.; Thornton, M.; Heidelberg, A.; Sheridan, J. G.; Blau, W.; Leahy, R. *J. Vac. Sci. Technol., B* **2006**, *24* (5), 2306−2311.

(6) Madaria, A. R.; Kumar, A.; Ishikawa, F. N.; Zhou, C. *Nano Res.* **2010**, *3* (8), 564−573.

(7) Ou, E. C. W.; Hu, L.; Raymond, G. C. R.; Soo, O. K.; Pan, J.; Zheng, Z.; Park, Y.; Hecht, D.; Irvin, G.; Drzaic, P.; Gruner, G. *ACS Nano* **2009**, *3* (8), 2258−2264.

(8) De, S.; Higgins, T. M.; Lyons, P. E.; Doherty, E. M.; Nirmalraj, P. N.; Blau, W. J.; Boland, J. J.; Coleman, J. N. *ACS Nano* **2009**, *3* (7), 1767−1774.

(9) Scardaci, V.; Coull, R.; Lyons, P. E.; Rickard, D.; Coleman, J. N. *Small* **2011**, *7* (18), 2621−2628.

(10) Gaynor, W.; Lee, J.-Y.; Peumans, P. *ACS Nano* **2009**, *4* (1), 30−34.

(11) Boland, J. J. *Nat. Mater.* **2010**, *9* (10), 790−792.

(12) Lipomi, D. J.; Vosgueritchian, M.; Tee, B. C. K.; Hellstrom, S. L.; Lee, J. A.; Fox, C. H.; Bao, Z. *Nat. Nanotechnol.* **2011**, *6* (12), 788−792.

(13) Takei, K.; Takahashi, T.; Ho, J. C.; Ko, H.; Gillies, A. G.; Leu, P. W.; Fearing, R. S.; Javey, A. *Nat. Mater.* **2010**, *9* (10), 821−826.

(14) Azulai, D.; Belenkova, T.; Gilon, H.; Barkay, Z.; Markovich, G. *Nano Lett.* **2009**, *9* (12), 4246−4249.

(15) White, S. I.; Mutiso, R. M.; Vora, P. M.; Jahnke, D.; Hsu, S.; Kikkawa, J. M.; Li, J.; Fischer, J. E.; Winey, K. I. *Adv. Funct. Mater.* **2010**, *20* (16), 2709−2716.

(16) Ling, Q.-D.; Liaw, D.-J.; Zhu, C.; Chan, D. S.-H.; Kang, E.-T.; Neoh, K.-G. *Prog. Polym. Sci.* **2008**, *33* (10), 917−978.

(17) Garnett, E. C.; Cai, W.; Cha, J. J.; Mahmood, F.; Connor, S. T.; Greyson Christoforo, M.; Cui, Y.; McGehee, M. D.; Brongersma, M. L. *Nat. Mater.* **2012**, *11* (3), 241−249.

(18) Rathmell, A. R.; Nguyen, M.; Chi, M. F.; Wiley, B. J. *Nano Lett.* **2012**, *12* (6), 3193−3199.

(19) Lee, T.; Chen, Y. *MRS Bull.* **2012**, *37* (02), 144−149.

(20) Scott, J. C.; Bozano, L. D. *Adv. Mater.* **2007**, *19* (11), 1452−1463.

(21) de Pablo, P. J.; Martínez, M. T.; Colchero, J.; Gómez-Herrero, J.; Maser, W. K.; Benito, A. M.; Muñoz, E.; Baró, A. M. *Adv. Mater.* **2000**, *12* (8), 573−576.

(22) Fujiwara, A.; Iijima, R.; Ishii, K.; Suematsu, H.; Kataura, H.; Maniwa, Y.; Suzuki, S.; Achiba, Y. *Appl. Phys. Lett.* **2002**, *80* (11), 1993−1995.

(23) Fujiwara, A.; Iijima, R.; Suematsu, H.; Kataura, H.; Maniwa, Y.; Suzuki, S.; Achiba, Y. *Physica B* **2002**, *323* (1−4), 227−229.

(24) Rispal, L.; Stefanov, Y.; Wessely, F.; Schwalke, U. *Jpn. J. Appl. Phys.* **2006**, *45*, 3672−3679.

(25) Stadermann, M.; Papadakis, S. J.; Falvo, M. R.; Fu, Q.; Liu, J.; Fridman, Y.; Boland, J. J.; Superfine, R.; Washburn, S. *Phys. Rev. B* **2005**, *72* (24), 245406.

(26) Stadermann, M.; Papadakis, S. J.; Falvo, M. R.; Novak, J.; Snow, E.; Fu, Q.; Liu, J.; Fridman, Y.; Boland, J. J.; Superfine, R.; Washburn, S. *Phys. Rev. B* **2004**, *69* (20), 201402.

(27) Nirmalraj, P. N.; Lyons, P. E.; De, S.; Coleman, J. N.; Boland, J. J. *Nano Lett.* **2009**, *9* (11), 3890−3895.

(28) Nirmalraj, P. N.; Lutz, T.; Kumar, S.; Duesberg, G. S.; Boland, J. J. *Nano Lett.* **2011**, *11* (1), 16−22.

(29) Nirmalraj, P. N.; Boland, J. J. *ACS Nano* **2010**, *4* (7), 3801−3806.

(30) Colvin, J. *EOS/ESD Symp. Proc.* **1990**, EOS-12, 173−174.

(31) Jo, S. H.; Chang, T.; Ebong, I.; Bhadviya, B. B.; Mazumder, P.; Lu, W. *Nano Lett.* **2010**, *10* (4), 1297−1301.

(32) Zamarreño-Ramos, C.; Camuñas-Mesa, L. A.; Pérez-Carrasco, J. A.; Masquelier, T.; Serrano-Gotarredona, T.; Linares-Barranco, B. *Front. Neurosci.* **2011**, *5*, 26.

(33) Waser, R.; Aono, M. *Nat. Mater.* **2007**, *6* (11), 833−840.

(34) Kim, Y. S.; Kim, J. S.; Choi, J. S.; Hwang, I. R.; Hong, S. H.; Kang, S. O.; Park, B. H. *Appl. Phys. Lett.* **2011**, *98* (19), 192104−3.